eLIFE elifesciences.org

RESEARCH ARTICLE

Figures and figure supplements

Sensory experience inversely regulates feedforward and feedback excitation-inhibition ratio in rodent visual cortex

Nathaniel J Miska *et al*

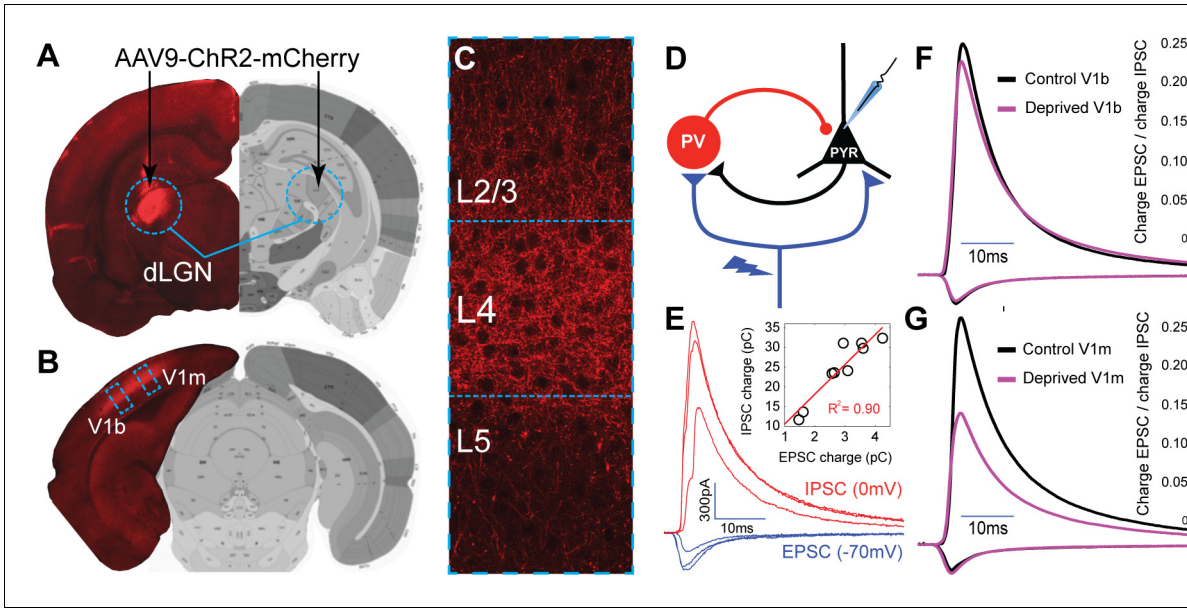

Figure 1. Brief MD increases thalamocortical-evoked Excitation-Inhibition (**E–I**) ratio in V1m. (**A**) Stereotaxic injection of AAV-ChR2-mCherry into dLGN (red) (**B**) leads to reporter expression within thalamocortical axons in V1m and V1b, (**C**) with densest innervation in layer 4 (**L4**). (**D**) Layer 4 pyramidal neurons were voltage-clamped in normal ACSF while stimulating local ChR2-mCherry+ thalamocortical axons with 473 nm light. (**E**) Representative example traces from a single neuron): brief (2 ms) stimuli were given at increasing laser intensity while alternating between the experimentally determined inhibitory and excitatory reversal potentials (−70 mV and 0 mV, respectively) to record paired monosynaptic thalamocortical-evoked EPSCs and disynaptic thalamocortical-evoked IPSCs. Inset: EPSC charge plotted versus IPSC charge for individual E-I pairs from this example neuron, with linear fit plotted in red (R^2 = 0.90). (**F**) Mean EPSC charge-normalized EPSC and IPSC traces for control (black) and deprived (magenta) neurons within V1b. Inset: Mean E-I charge ratio for control (black) and deprived (magenta) neurons (control n = 14 neurons, deprived n = 30 neurons, from six animals; p = 0.80, 2-sample t-test). (**G**) Same as F), but for neurons within V1m. Inset: Mean E-I charge ratio for control (black) and deprived (magenta) neurons (control n = 14 neurons, deprived n = 11 neurons, from seven animals; p = 0.0063, 2-sample t-test). Atlas images in A) and B) adapted from Allen Mouse Brain Atlas (***Dong, 2008***).

DOI: https://doi.org/10.7554/eLife.38846.002

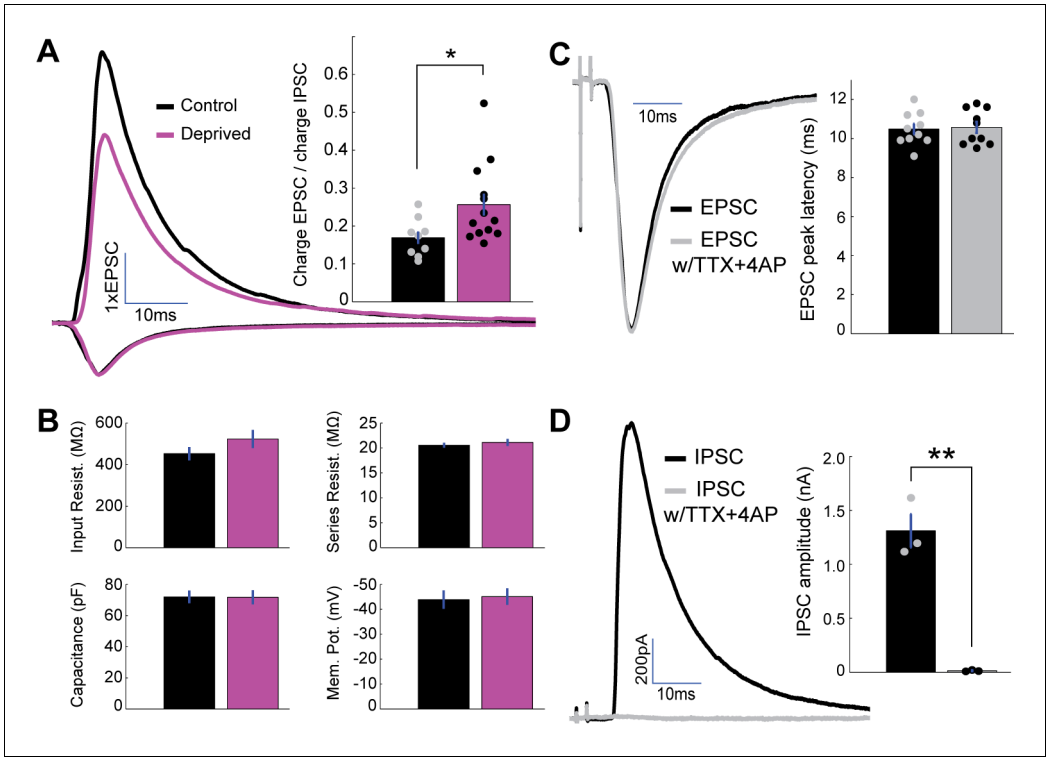

Figure 1—figure supplement 1. Measuring thalamocortical E-I ratio. (**A**) Mean EPSC charge-normalized E and I traces for control (black) and deprived (magenta) neurons. Inset: Mean E-I charge ratio for control (black) and deprived (magenta) neurons. (control n = 9, deprived n = 13, from 9 Long-Evans rats, p = 0.032, 2-sample t-test). (**B**) Mean input resistance, series resistance, capacitance, and resting membrane potential for control (black) and deprived (magenta) neurons. (**C**) Mean peak-scaled thalamocortical EPSCs evoked in regular ACSF (black) and following perfusion of TTX+4-AP (grey). Bar plot: EPSC peak latency in regular ACSF (black) and following perfusion of TTX+4-AP (grey) (n = 10, p = 0.82, 2-sample t-test). (**D**) Mean thalamocortical IPSCs evoked in regular ACSF (black) and following perfusion of TTX+4-AP (grey). Bar plot: IPSC amplitude in regular ACSF (black) and following perfusion of TTX+4-AP (grey) (n = 3, p = 0.0014, 2-sample t-test).

DOI: https://doi.org/10.7554/eLife.38846.003

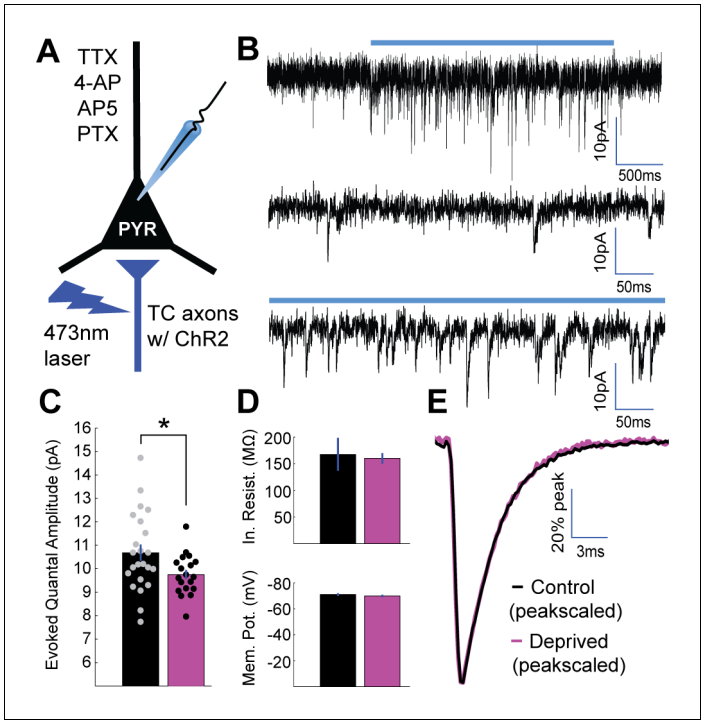

Figure 2. Brief MD reduces thalamocortical quantal amplitude onto layer 4 pyramidal neurons. (**A**) Whole-cell recordings were obtained from layer 4 pyramidal neurons in V1m in a drug cocktail of TTX, 4-AP, AP5, and PTX to isolate excitatory quantal events while stimulating local ChR2-mCherry+ thalamocortical (TC) axons (red) with 473 nm light. (**B**) Top: example recording of quantal events during 2 s laser stimulation (blue bar). Middle: Pre-stimulus spontaneous mEPSCs. Bottom: Evoked quantal events during laser stimulation. (**C**) Mean evoked quantal amplitudes for control (black) and deprived (magenta) neurons (control n = 23 neurons deprived n = 19 neurons, from 15 animals; p = 0.033, 2-sample t-test). (**D**) Mean input resistance (top) and resting membrane potential (bottom) for control and deprived neurons. (**E**) Overlaid peak-scaled evoked event waveform averages for control (black) and deprived (magenta) neurons, to illustrate kinetics. For all bar plots here and below, circles represent individual values, and error bars indicate ±SEM.

DOI: https://doi.org/10.7554/eLife.38846.005

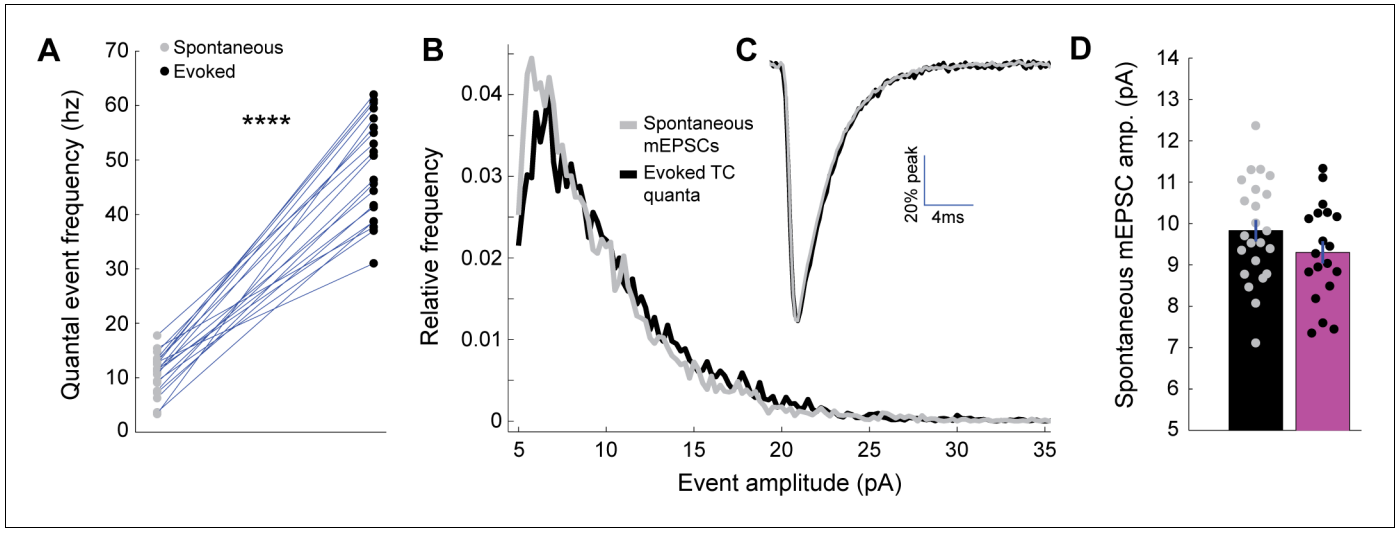

Figure 2—figure supplement 1. Evoked thalamocortical quantal events and spontaneous mEPSCs show similar amplitude distributions and event kinetics. (**A**) Spontaneous mEPSC frequency (grey) and evoked mEPSC frequency (black) for a random subset of manually analyzed neurons, with lines connecting spontaneous and evoked values for each neuron (n = 20 neurons, $p = 5.5\times10^{-19}$, 2-sample t-test). (**B**) Mean normalized event amplitude histogram for all neurons, with stimulus-evoked thalamocortical quantal events plotted in black and spontaneous mEPSCs in grey. (**C**) Peak-scaled mean event waveforms for thalamocortical quantal events (black) and spontaneous mEPSCs (grey), to illustrate kinetics. (**D**) Spontaneous mEPSC amplitudes measured for the same neurons as in ***Figure 1***, with control in black and deprived in magenta (control n = 23, deprived n = 19, p = 0.17, 2-sample t-test).

DOI: https://doi.org/10.7554/eLife.38846.006

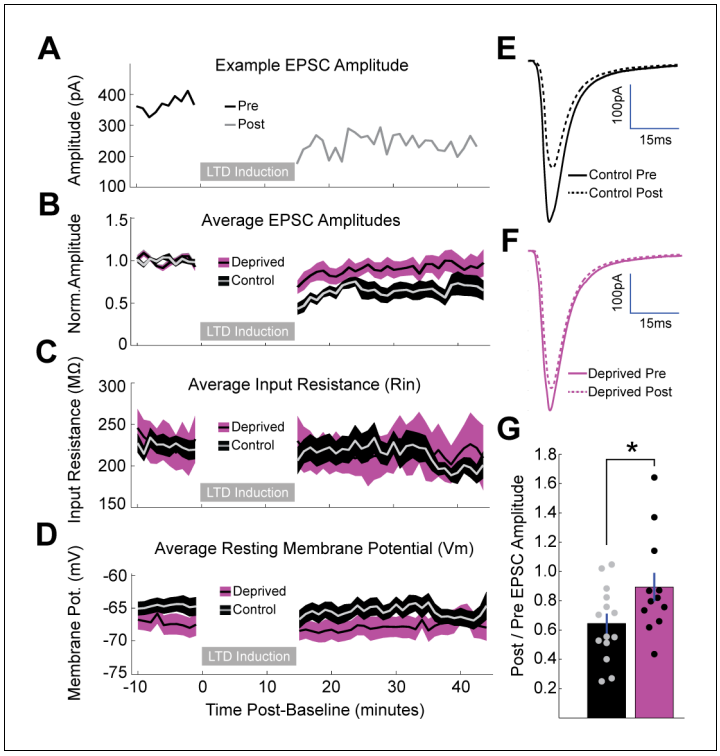

Figure 3. Brief MD occludes induction of LTD at thalamocortical synapses onto layer 4 pyramidal neurons. (**A**) Representative example of LTD induction from a nondeprived neuron in V1m, with pre-induction evoked EPSC amplitudes plotted in black, post-induction amplitudes plotted in grey, and LTD induction period represented as a grey bar. (**B**) Mean, baseline-normalized evoked EPSCs plotted for control (grey with black shading) and deprived (black with magenta shading) neurons. Shaded region represents SEM. (**C**) Mean input resistance (Rin) and (**D**) mean resting membrane potential (Vm) plotted for control and deprived neurons. (**E, F**) Average EPSC waveforms for control neurons (**E**) pre-induction (black, solid) and post-induction (black, dashed); and deprived neurons (**F**) pre-induction (magenta, solid) and post-induction (magenta, dashed). (**G**) Mean post/pre EPSC amplitude ratio for control (black) and deprived (magenta) neurons (control n = 14 neurons, deprived n = 12 neurons, from eight animals; p = 0.042, 2-sample t-test).

DOI: https://doi.org/10.7554/eLife.38846.008

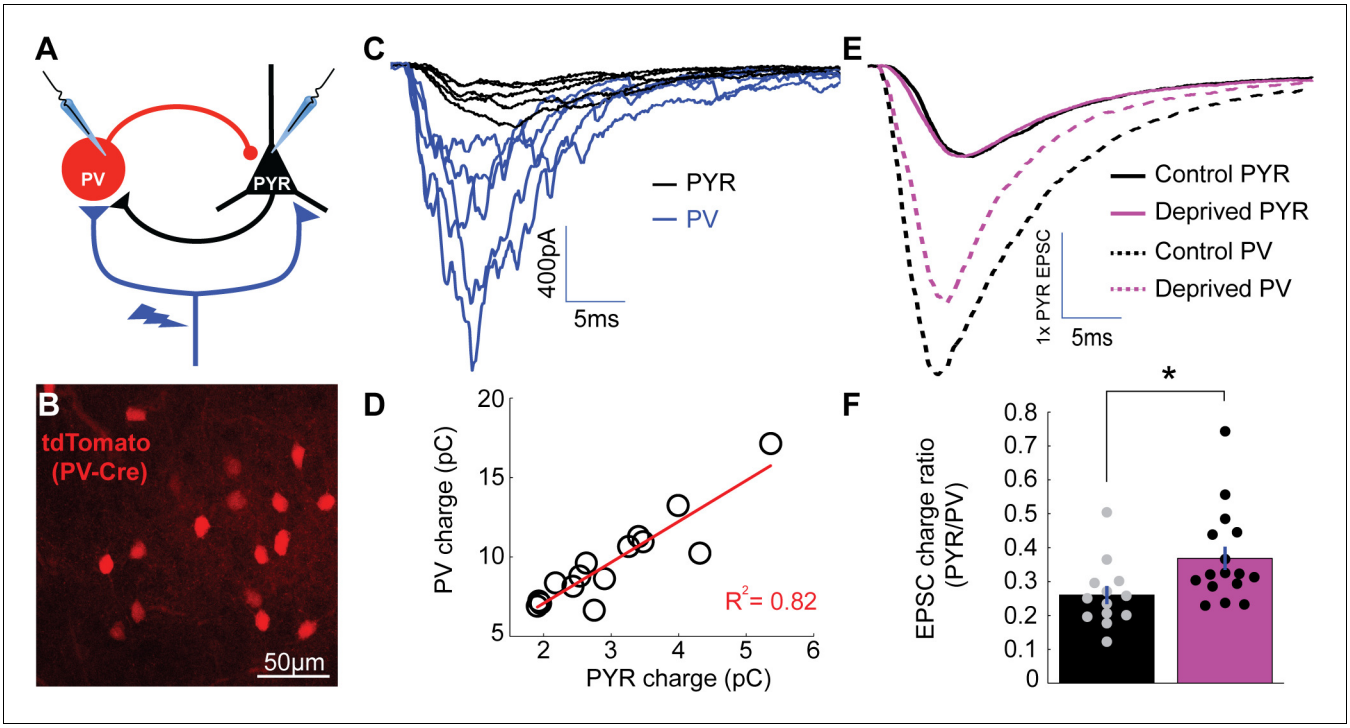

Figure 4. Enhanced depression at thalamocortical synapses onto PV+ interneurons following brief MD. (**A**) Whole-cell recordings were obtained from pairs of pyramidal neurons (black) and nearby PV+ interneurons (blue) within V1m while stimulating local ChR2-mCherry+ thalamocortical axons (red). (**B**) PV+ interneurons were targeted by reporter (tdTomato) expression. (**C**) Representative example traces from a pyramidal and PV pair while stimulating thalamocortical axons at a range of stimulus intensities, with pyramidal traces in black (PYR) and PV+ interneuron traces in blue (PV). Note the larger thalamocortical EPSCs in the PV+ interneuron compared to the pyramidal neuron. (**D**) Charge of thalamocortical EPSCs in the pyramidal neuron plotted against corresponding thalamocortical EPSCs in the PV+ interneuron. Linear fit plotted in red (R^2 = 0.82). (**E**) Averaged traces from all pairs (control in black and deprived in magenta) normalized to pyramidal EPSC peak amplitude. (**F**) Evoked thalamocortical EPSC charge ratio (PYR/PV) for control (black) and deprived (magenta) pairs (control n = 13 pairs, deprived n = 16 pairs, from 13 animals; p = 0.0103, Wilcoxon rank sum test).
DOI: https://doi.org/10.7554/eLife.38846.010

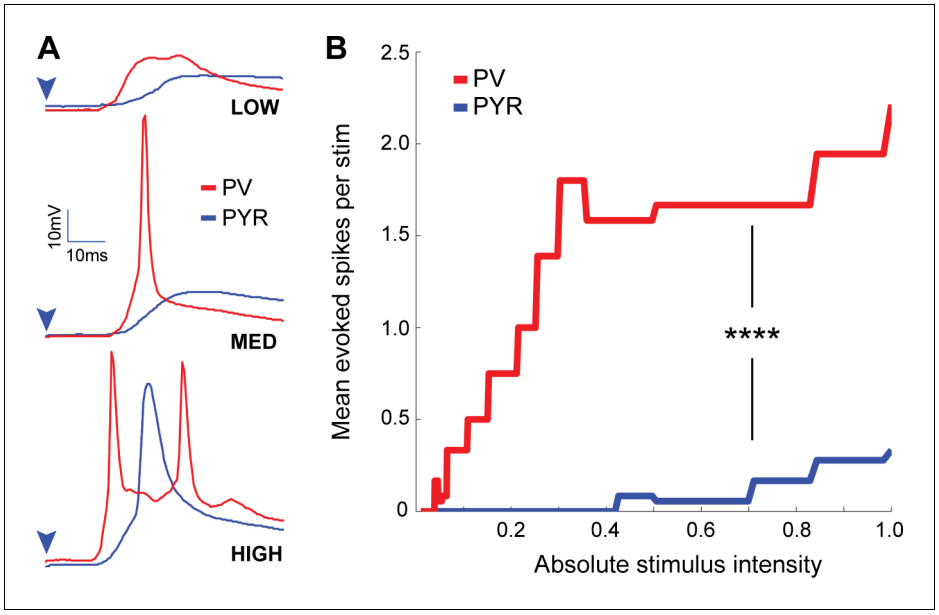

Figure 4—figure supplement 1. PV+ interneurons readily fire to thalamocortical stimulation, whereas pyramidal neurons do not. (**A**) Example traces from a paired recording between a PV+ interneuron (red) and nearby pyramidal neuron (blue) showing firing responses to low, medium, and high intensity optogenetic stimulation of thalamocortical afferents. (**B**) Mean evoked spikes for all PV+ interneurons (red) and pyramidal neurons (blue) versus laser stimulus strength (n = 6 pairs, $p = 2.3\times10^{-42}$ two-sample Kolmogorov-Smirnov test).
DOI: https://doi.org/10.7554/eLife.38846.011

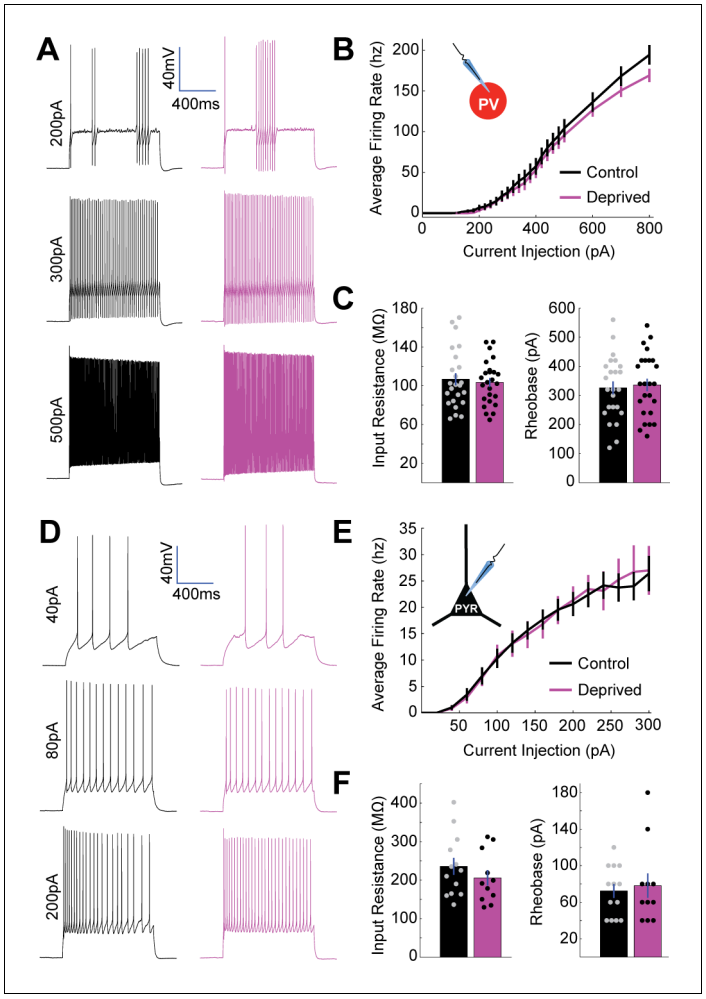

Figure 5. No change in intrinsic excitability of layer 4 PV+ interneurons or pyramidal neurons following brief MD. (**A**) Representative example traces from a control PV+ interneuron (black) and a deprived PV+ interneuron (magenta) in V1m showing firing responses to 1 s long current injections of 200 pA (top), 300 pA (middle), and 500 pA (bottom). (**B**) PV+ interneuron firing rate versus current injection (FI) plotted for all neurons in control (black, n = 24) or deprived (magenta, n = 25) conditions; data obtained from 10 animals. (**C**) Mean input resistance (left) and mean rheobase (right) for control (black) and deprived (magenta) PV+ interneurons. (**D**) Representative example traces from control (black) and deprived (magenta) layer 4 pyramidal neurons showing firing responses to 1 s long current injections of 40 pA (top), 80 pA (middle), and 200 pA (bottom). (**E**) Pyramidal neuron firing rate versus current injection (FI) plotted for all neurons in control (black, n = 13) or deprived (magenta, n = 11) conditions; data obtained from seven animals. (**F**) Mean input resistance (left) and mean rheobase (right) for control (black) and deprived (magenta) pyramidal neurons.

DOI: https://doi.org/10.7554/eLife.38846.013

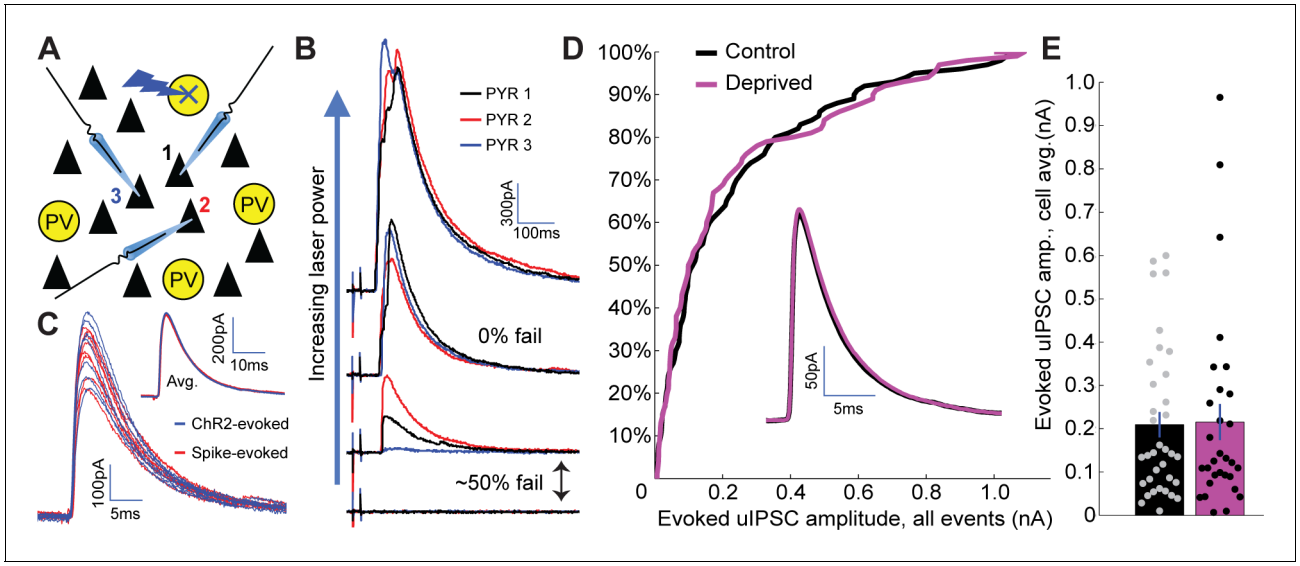

Figure 6. No change in PV+ interneuron to pyramidal neuron inhibitory synaptic strength following brief MD. (**A**) Recording/stimulating configuration. While recording from multiple pyramidal neurons within V1m, nearby PV+ interneurons expressing ChR2-YFP were targeted serially with focal laser stimulation. (**B**) For each targeted PV+ interneuron, laser stimulation strength was initially very low and was gradually increased until one or more recorded pyramidal neurons exhibited ~50% rate of failure in evoked IPSCs. (**C**) Example IPSCs evoked using optogenetic stimulation (blue) or by patching the same PV+ interneuron and evoking individual spikes with current injection (red). Inset: average traces from each method overlaid. (**D**) Cumulative probability distribution for all putative unitary IPSC amplitudes (includes multiple inputs per pyramidal neuron) is not significantly different between control and deprived conditions (control n = 68, deprived n = 59, from 11 animals; p = 0.90, two-sample Kolmogorov-Smirnov test). Inset: average IPSC waveforms (cell-averages) are indistinguishable between control and deprived pyramidal neurons. (**E**) Quantification of cell-averaged putative unitary IPSC amplitudes shows no significant difference between control and deprived pyramidal neurons (control amplitude = 209 ± 29 pA n = 35 neurons, deprived amplitude = 215 ± 42 pA n = 30 neurons, p = 0.73, Wilcoxon rank sum test).

DOI: https://doi.org/10.7554/eLife.38846.015

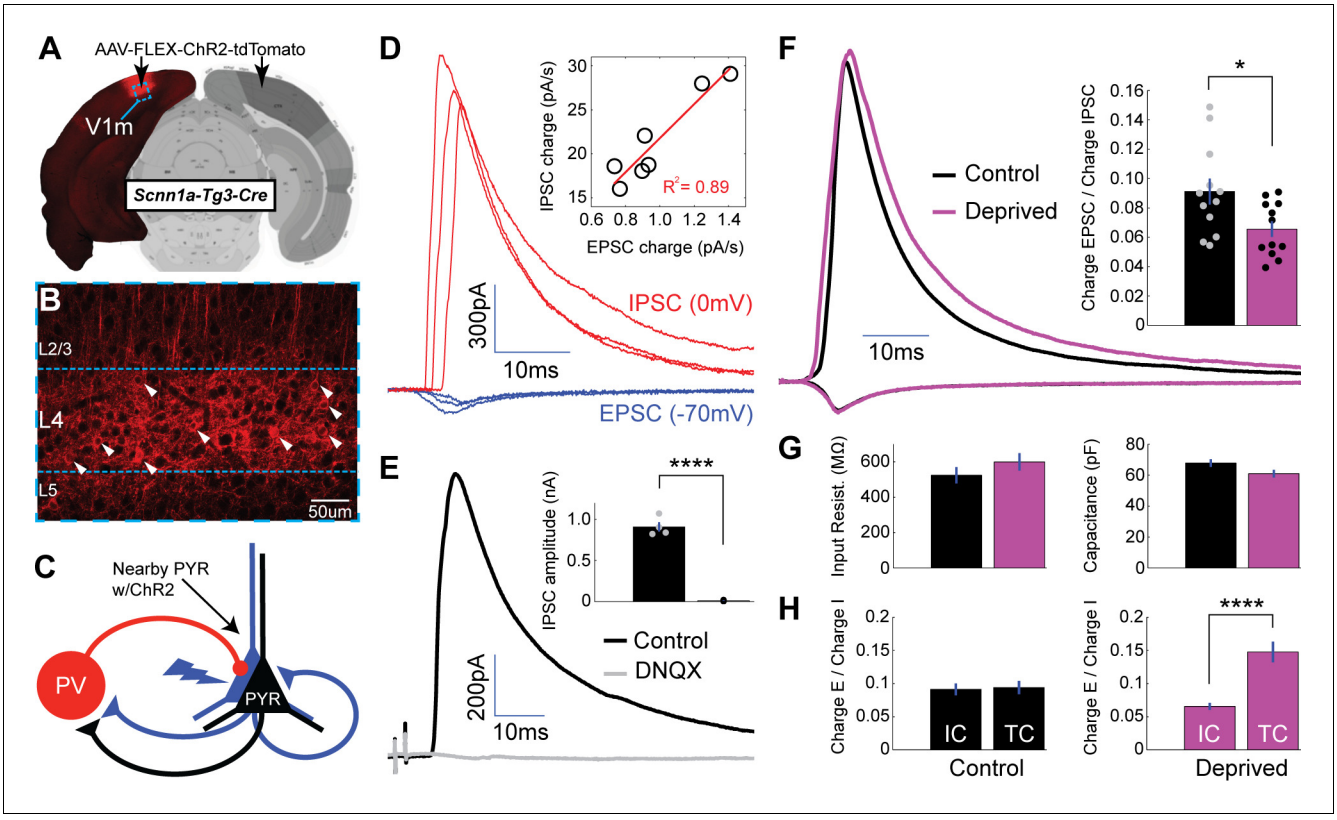

Figure 7. Local intracortical-evoked E-I ratio shifts toward inhibition following brief MD. (**A**) Cre-dependent ChR2-tdTomato expression (red) from stereotaxic injection of AAV into V1m of Scnn1a-Tg3-Cre mice. (**B**) Confocal image from site of viral infection, with infected layer 4 pyramidal neurons marked with white arrows. (**C**) Diagram of recording configuration: whole-cell recordings were obtained from uninfected layer 4 pyramidal neurons while stimulating neighboring ChR2-tdTomato+ pyramidal neurons with brief (2 ms) pulses of 473 nm light. (**D**) Representative example paired EPSCs (red) and IPSCs (blue) recorded at experimentally verified reversal potentials (−70 mV and 0 mV) at several stimulus intensities. Inset: EPSC versus IPSC charge elicited by a range of stimulus intensities for a single neuron, with linear fit plotted in red (R^2 = 0.89). (**E**) Evoked IPSCs in regular ACSF (black) and following perfusion of DNQX (grey) (n = 4). (**F**) Mean EPSC charge-normalized EPSC and IPSC traces for control (black) and deprived (magenta) neurons. Right: Mean E-I charge ratio for control (black) and deprived (magenta) neurons (control n = 12, deprived n = 12, from eight animals; p = 0.022, 2-sample t-test). (**G**) Mean input resistance and capacitance for control (black) and deprived (magenta) neurons. (**H**) Left: control intracortical (IC) versus thalamocortical (TC) E-I ratios (p = 0.84, 2-way t-test). Right: deprived intracortical versus thalamocortical E-I ratios (p = 4.1×10^{-5}, 2-sample t-test). Atlas image in A) adapted from Allen Mouse Brain Atlas (***Dong, 2008***).

DOI: https://doi.org/10.7554/eLife.38846.017

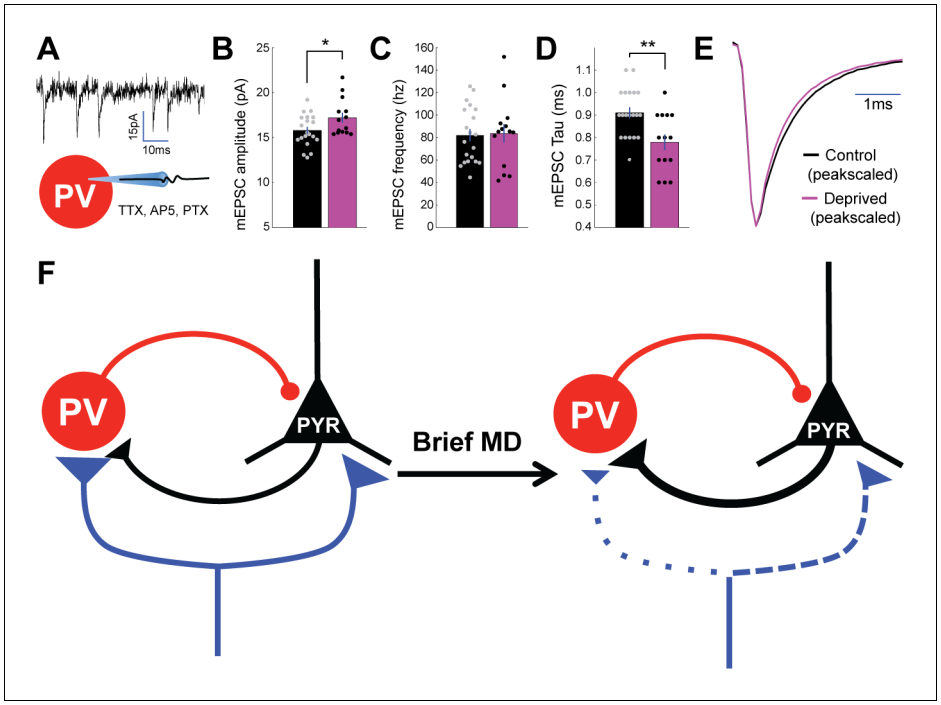

Figure 8. Spontaneous mEPSC amplitude onto PV+ interneurons is enhanced by brief MD. (**A**) Whole cell recordings were performed in V1m on PV+ interneurons in TTX, AP5, and PTX to isolate spontaneous mEPSCs. (**B**) Quantification of mEPSCs shows a significant potentiation in amplitude following brief MD ($p = 0.044$, Wilcoxon rank sum test), (**C**) no change in event frequency ($p = 0.86$, 2-sample t-test), and (**D**) a significant decrease in event decay constant ($p = 0.003$, 2-sample t-test. Control $n = 20$, deprived $n = 14$, from 10 animals). (**E**) Average mEPSC waveforms (left) and peak-scaled average mEPSC waveforms (right) for interneurons from control (black) and deprived (magenta) hemispheres. (**F**) Scheme summarizing changes within layer 4 circuit following brief MD, with synapse size and line width corresponding to synaptic strength and dotted lines specifically indicating weaker synaptic strength. Specifically, MD leads to depression of thalamocortical strength onto both pyramidal neurons and PV+ interneurons, though this depression is greater onto PV+ interneurons. MD also strengthens excitatory connections from pyramidal neurons to PV+ interneurons.

DOI: https://doi.org/10.7554/eLife.38846.019

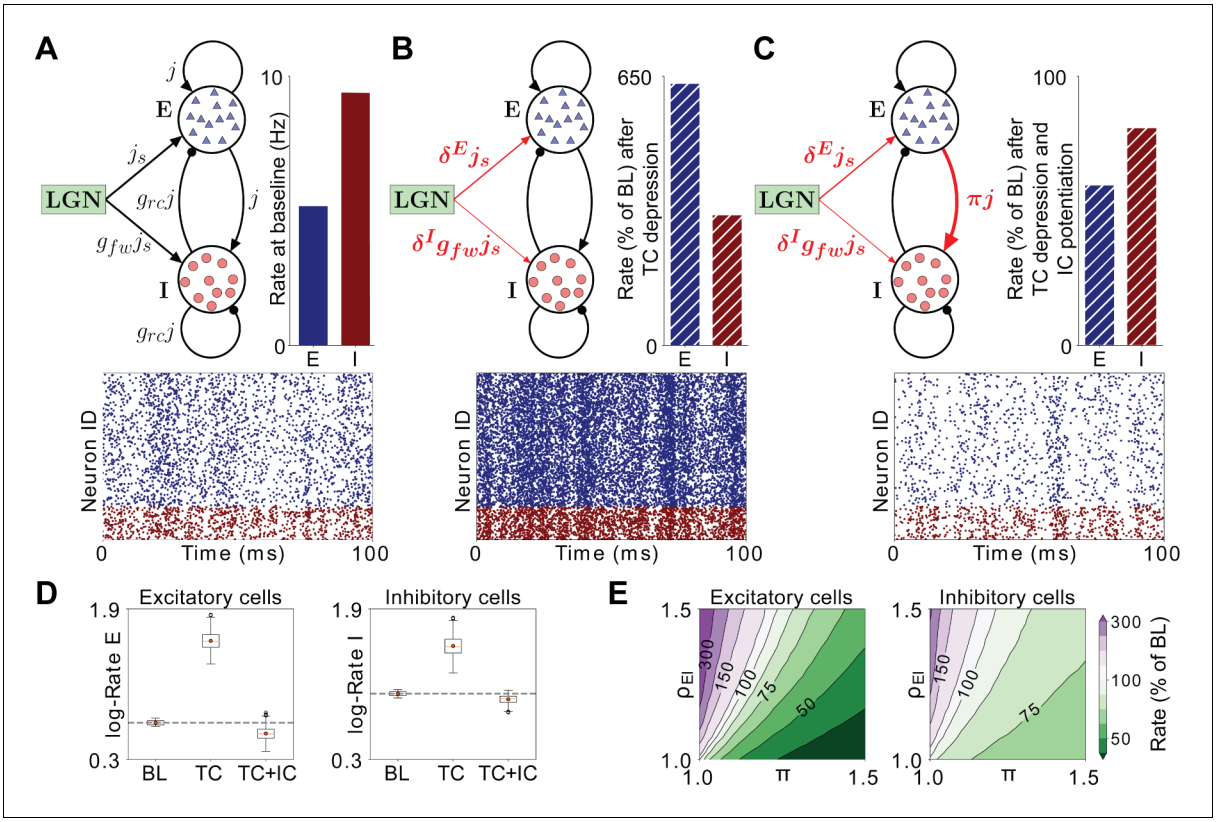

Figure 9. Firing rates in a model layer 4 circuit incorporating MD-induced synaptic changes in V1m. (**A**) Schematic of the network model under baseline conditions. All excitatory synaptic weights in the network are given by the parameter j, and inhibitory connections are further scaled with a factor g_{rc}. Excitatory neurons receive thalamic input with synaptic weight j_s, while the stronger thalamic input onto inhibitory neurons is captured by multiplying j_s with the factor $g_{fw} > 1$. Bar plot: Firing rates of excitatory (E, red) and inhibitory (I, blue) neurons in the model at baseline (BL). Raster plot: Representative spiking activity across neurons over 100 ms at BL. (**B**) Schematic of the network model after implementing synaptic depression in thalamocortical (TC) projections onto excitatory neurons (δ^E) and greater depression onto inhibitory neurons (δ^I). Bar plot: firing rates as a percentage of BL resulting from these synaptic changes. Raster plot: representative spiking activity across neurons over 100 ms after implementing TC depression. (**C**) Same as B), but with the addition of intracortical (IC) potentiation (π) of recurrent excitatory drive to inhibitory neurons (TC + IC). (**D**) Box plots of the firing rates in 2491 implementations of the network with randomly chosen parameters, simulated at BL, after TC depression and after TC depression and IC potentiation. The boxplots show the interquartile range (IQR) of the simulated firing rates (red symbol denotes the mean, red line denotes the median), with the whiskers denoting ± 1.5 IQR. Outliers (black circles) are firing rates beyond the ± 1.5 IQR. Rates are shown on a logarithmic scale for excitatory neurons (left panel) and inhibitory neurons (right panel). (**E**) Combined effects of increased TC E-I ratio (ρ_{EI}) and potentiation of recurrent excitatory drive to inhibition (π) on firing rates of excitatory (left panel) and inhibitory neurons (right panel). Firing rates are shown as percentage of BL for all combinations of π and ρ_{EI}. Green-shifted color regions represent lower rates and purple-shifted regions represent higher rates relative to BL.

DOI: https://doi.org/10.7554/eLife.38846.021